# The mitotic role of Adenomatous Polyposis Coli requires its bilateral interaction with tubulin and microtubules

Laurence Serre, Julie Delaroche, Angélique Vinit, Guy Schoehn, Eric Denarier, Anne Fourest-Lieuvin, Isabelle Arnal

Journal of Cell Science

# Author queries: JCS260152

Please indicate your corrections using comments/annotations as shown in the corrected proof example (please do not use the 'sticky notes' tool or edit the text directly).

Please check the **entire proof** thoroughly, paying particular attention to any text highlighted in red.
Check carefully that the authors' names, affiliations and the corresponding author's e-mail address are correct.
Please ensure that all tables, figures and equations are present and in the correct order.

**IMPORTANT:** If you submit revised figures, please let us know what has been changed in the figures so that we can check that the files have been substituted in the final proof.

**Funding:** The funding data linked to your article are summarised in a table at the end of the proof. **Please check that all funders and institutions supporting your work and relevant grant numbers are included.** Funder names may have been edited to match the Crossref Open Funder Registry. Note that this table will not be included in your published paper.

**PubMed Central deposition/Self-archiving:** We offer a free PMC deposition service to authors supported by funders that mandate deposition in US/NLM PMC. If you require deposition and this is not indicated in the Funding section of your proof (Deposited in PMC for release…), please let us know immediately. For deposition in other publicly available repositories, see Open Access rights and permissions.

**Gold Open Access - CC-BY:** If you have paid for Gold Open Access publication, the CC-BY licence text will be displayed on page 1 of your proof, below the author affiliations. Open access papers will be deposited in US/NLM PMC for immediate release. Note that all other papers will be published under our Green Open Access model free of charge, and made freely available 6 months after publication. For further details, see Open Access rights and permissions.

**Supplementary information:** If you have submitted supp. data, please check that citations are included in the text. Please note there are no proofs for supp. data as the files are not edited. If you wish to make any changes, please provide replacement file(s) and let us know what has been changed.

## Please answer the hyperlinked queries below and indicate any necessary changes on the proof.

AQ1 JCS plays an active role in increasing the visibility of your paper. To help us promote your article on social media, please provide the Twitter handle of the corresponding author and first author, and primary institution at which the work was conducted. For further ways that you can help your paper reach a wider audience, see the guidelines on our website.

AQ2 Please provide department name in affiliations (1, 2) if applicable, and postal code in affiliations (1, 2).

AQ3 Past tense is used for results from the present study, with present tense for results from previous studies (present tense is also fine in the conclusion and summary sections). Some edits have been made to this effect.

AQ4 Please check that the edits here from 'amino acid sequence of APC-C' to 'electron density of APC-C' are scientifically accurate.

AQ5 Where possible, we try to avoid having paragraphs containing only one sentence and have removed some line breaks. Please check.

AQ6 Westermann et al. (2005) is not listed in the reference list. Please provide complete publication details to insert in the list, else delete text citation.

AQ7 Please provide details of the source of the indicated plasmid. If from Addgene, please also provide the plasmid number. If it was a gift, please indicate the name and affiliation of the scientist.

AQ8 Please provide a brief summary of the experimental protocol used here.

AQ9 Please provide supplier details for reagents where indicated.

AQ10 Please provide the centrifugation speed in g.

AQ11 Could you please clarify what '(2-28)' is referring to here?

AQ12 Could '1/10 nm' and '1/4 nm' be written as '0.1 nm' and '0.25 nm', respectively?

AQ13 Please specify the dilutions used, catalogue numbers and supplier details for antibodies where indicated.

AQ14 Please clarify what 'α3-a1' represents.

AQ15 A search for '80466, BioValley' does not provide any relevant results. Could you please check the supplier details for these dishes?

AQ16 Journal of Cell Science uses the CRediT Taxonomy to define author contributions to primary research papers. Details for this section are taken from those provided at submission. Please check carefully.

AQ17 Please check the funding section. Funders may have been edited in order to exactly match the CrossRef funder registry (http://search.crossref.org/fundref). Note that the funding table at the end of your proof will be deleted before publication but both the table and the Funding section must be correct.

AQ18 The Data Availability section is intended for high-throughput datasets that have been submitted to repositories. Please deposit and make publicly accessible the cryo-electron microscopy data generated in this study to the Electron Microscopy Data Bank (EMDB), and provide accession numbers here. For more information, see our Data deposition policy.

AQ19 Reference Beckers and Sachse (2020) is listed in the reference list but not cited in the text. Please cite in the text, else delete from the list.

AQ20 The star does not appear to be shown in Fig. 2F. Please provide a new figure containing a clearly marked star.

AQ21 Where images are shown, please specify how many experiments these are representative of.

AQ22 The text 'metaphase alignment' in the lower left panel of Fig. 6A is spilling over to the adjoining panel. Could you please adjust this text and provide a new figure?

AQ23 The *P*-value for '*' has been removed as it is not shown in Fig. 6B,C. Please check.

AQ24 Please check that the table is formatted correctly.

AQ25 Please check that the summary statement provides an accurate and representative outline of your study. It may have been edited to include additional information not apparent from the title and to comply with the limit of about 200 characters.

© 2023. Published by The Company of Biologists Ltd | Journal of Cell Science (2022) 136, jcs260152. doi:10.1242/jcs.260152

RESEARCH ARTICLE

# The mitotic role of adenomatous polyposis coli requires its bilateral interaction with tubulin and microtubules

**Laurence Serre[1,‡], Julie Delaroche[1], Angélique Vinit[1,*], Guy Schoehn[2], Eric Denarier[1], Anne Fourest-Lieuvin[1] and Isabelle Arnal[1,‡]**

AQ1: AQ1:

## ABSTRACT

Adenomatous polyposis coli (APC) is a scaffold protein with tumour suppressor properties. Mutations causing the loss of its C-terminal domain (APC-C), which bears cytoskeleton-regulating sequences, correlate with colorectal cancer. The cellular roles of APC in mitosis are widely studied, but the molecular mechanisms of its interaction with the cytoskeleton are poorly understood. Here, we investigated how APC-C regulates microtubule properties, and found that it promotes both microtubule growth and shrinkage. Strikingly, APC-C accumulates at shrinking microtubule extremities, a common characteristic of depolymerases. Cryo-electron microscopy revealed that APC-C adopts an extended conformation along the protofilament crest and showed the presence of ring-like tubulin oligomers around the microtubule wall, which required the presence of two APC-C sub-domains. A mutant of APC-C that was incapable of decorating microtubules with ring-like tubulin oligomers exhibited a reduced effect on microtubule dynamics. Finally, whereas native APC-C rescued defective chromosome alignment in metaphase cells silenced for APC, the ring-incompetent mutant failed to correct mitotic defects. Thus, the bilateral interaction of APC-C with tubulin and microtubules likely contributes to its mitotic functions.

**KEY WORDS: APC, Microtubule, Tubulin, Depolymerase, Mitosis**

## INTRODUCTION

Adenomatous polyposis coli (APC) is a 340-kDa scaffold protein with tumour suppressor properties. Mutations in the *APC* gene correlate with the development of cancers, mostly colorectal cancers (Juanes, 2020; Näthke, 2006). The central portion of the *APC* gene is particularly sensitive to mutations producing premature termination of translation, resulting in truncated proteins. These short forms of APC lack the C-terminal domain, which is mainly responsible for interactions with the cytoskeleton (Moseley et al., 2007; Nakamura et al., 2001). Similar mutations have also been observed within the *APC2* gene, the neuronal isoform of *APC*, and are associated with cytoskeleton defects such as inadequate dendritic spine morphology or axon misguidance in neuronal disorders linked to Sotos syndrome or autism (Almuriekhi et al., 2015; Mohn et al., 2014; Onouchi et al., 2014).

Several studies have focused on the C-terminal domain of APC, called APC-C (residues 2131–2843), and highlighted its importance with regard to microtubule and actin regulation (Deka et al., 1998; Okada et al., 2010). APC-C was found to contain a basic domain that interacts with microtubules or actin monomers, alongside a dimerisation domain essential for actin nucleation (Okada et al., 2010) that overlaps with the binding site for neuronal kinesins (Ruane et al., 2016). It also contains distinct binding sites for other cytoskeleton-related proteins, including end-binding (EB) proteins (Honnappa et al., 2005; Serre et al., 2019) or the mitochondrial kinesin-motor complex Miro/Milton (Mills et al., 2016). The biological functions of the C-terminal domain of APC must be deciphered if we are to understand its cellular functions. This knowledge will shed light on the dysfunction of its truncated forms in cancers and neuronal pathologies, and in particular on how these mutations affect microtubule architecture and regulation during cell division (Bahmanyar et al., 2009; Fodde et al., 2001a; Rusan and Peifer, 2008). Indeed, we have found few molecular studies into the effects of APC on microtubule organisation and dynamics. To fill this gap, we combined a set of *in vitro* reconstitution and cellular approaches to characterise the microtubule regulatory properties of the C-terminal domain of APC. We found that APC-C stimulates both growth and shrinkage rates at microtubule minus and plus ends. Like other depolymerases (Brouhard et al., 2008; Tan et al., 2006), APC-C accumulates at the end of depolymerising microtubules. Using cryo-electron microscopy and image analysis, we observed APC-C bound to the surface of microtubules, where it adopted an extended conformation along protofilaments. Strikingly, APC-C was also seen to organise soluble tubulin as ring-like oligomers around the microtubule wall. A mutant incapable of decorating microtubules with these ring-like structures and exhibiting reduced effects on microtubule dynamics was unable to rescue chromosome alignment defects in metaphase cells silenced for APC, whereas complementation with APC-C did rescue these defects. Taken together, our results allowed us to develop a molecular model linking the role of APC in regulating microtubule dynamics and organisation to its function in mitosis.

## RESULTS

### The C-terminal domain of APC increases growth and shrinkage rates at microtubule ends

We first characterised the effect of purified APC-C (Fig. 1A) on microtubule assembly and disassembly using total internal reflection fluorescence (TIRF) microscopy. In our experimental conditions, the addition of 50 nM APC-C significantly increased both polymerisation and depolymerisation rates for microtubules (Fig. 1B,C; Fig. S1; Table 1; Movie 1). Thus, microtubule plus-ends

AQ2: [1]Université Grenoble Alpes, Inserm U1216, CEA, CNRS, Grenoble Institut Neurosciences, GIN, Grenoble, France. [2]Université Grenoble Alpes, CEA, CNRS, IBS, Grenoble, France.
*Present address: Université Sorbonne, Faculté de Médecine Pitié-Salpetrière, Paris, France.

‡Authors for correspondence (laurence.serre@univ-grenoble-alpes.fr, isabelle.arnal@univ-grenoble-alpes.fr)

L.S., 0000-0002-6794-1492; J.D., 0000-0003-2529-0270; A.V., 0000-0003-3344-4911; G.S., 0000-0002-1459-3201; E.D., 0000-0002-4169-397X; A.F., 0000-0003-1325-6788; I.A., 0000-0001-6149-8189

**Handling Editor: David Glover**
**Received 21 April 2022; Accepted 13 December 2022**

Journal of Cell Science (2022) 136, jcs260152. doi:10.1242/jcs.260152

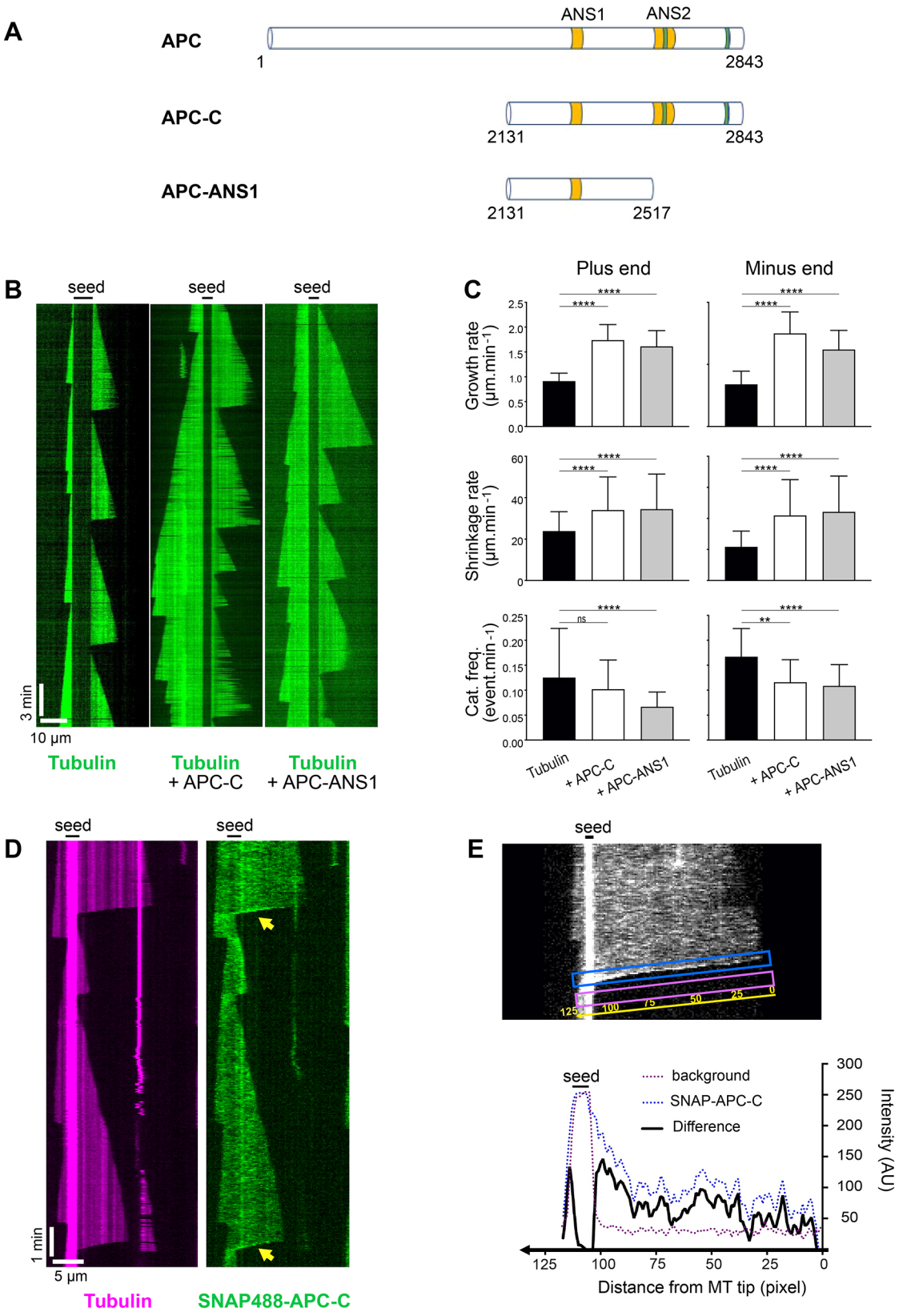


**Fig. 1.** See next page for legend.

grew twice as fast and depolymerised 30% faster in the presence of 50 nM APC-C. In addition, APC-C increased the rescue frequency and slightly decreased the catastrophe frequency. Similar effects of APC-C were observed at microtubule minus ends, with a 50% increase in both microtubule growth and shrinkage rates (Fig. 1C; Fig. S1; Table 1). A truncated form of APC-C (APC-ANS1),

**Fig. 1. The C-terminal domain of APC increases the growth and shrinkage rates of microtubules and accumulates at the ends of depolymerising microtubules.** (A) Schematic representation of the full-length APC and protein constructs used in this study. The regions marked in yellow indicate ANS1, a region involved in microtubule interaction, and ANS2, a dimerisation site – both domains are involved in actin nucleation. The regions marked in green indicate SxIP EB-binding sites. (B) Representative kymographs for microtubules grown with 15 µM tubulin alone (left) or with 50 nM APC-C (centre) or APC-ANS1 (right). (C) Growth rate, shrinkage rate and catastrophe frequency of the plus and minus ends of microtubules assembled in the absence or in the presence of APC-C. ns, not significant; $^{**}P<0.01$; $^{****}P<0.0001$ (Kruskal–Wallis test with Dunn's multiple comparisons). Data are represented as mean±s.d. Detailed values are given in Table 1 and SuperPlot representation of the data in Fig. S1. (D) Representative kymographs of microtubules grown with 15 µM tubulin (magenta) and 12 nM SNAP-488–APC-C (green), showing the accumulation of SNAP-488–APC-C at the extremities of depolymerising microtubules (yellow arrows). (E) Representative kymograph (top) and the corresponding intensity plot profile (bottom) of SNAP-488–APC-C measured along the microtubule depolymerizing end. The dashed blue line indicates SNAP-488–APC-C intensity along the microtubule end centred on the blue box in the kymograph. The dashed pink line indicates the background corresponding to the intensity measured along a line centred on the pink box in the kymograph. The plain black line indicates SNAP-488–APC-C intensity after subtraction of the background, allowing the removal of the signal of SNAP-488–APC-C that binds to the seed. AU, arbitrary units; MT, microtubule.

lacking the dimerisation domain (ANS2) and EB-binding sites, but including the ANS1 domain known to be involved in microtubule binding (Fig. 1A), had a similar effect on microtubule dynamics compared to APC-C (Fig. 1B,C; Fig. S1; Table 1). Therefore, APC-C appears to modulate microtubule dynamics at both ends through elements in its basic domain, not involving its dimerisation or EB-binding sites.

### The C-terminal domain of APC accumulates at the ends of depolymerising microtubules

Using a fluorescent form of APC-C (SNAP488–APC-C), we investigated whether the effects induced by APC-C on microtubule dynamics were associated with a specific distribution along or at the ends of growing and shrinking microtubules. Inspection of the kymographs obtained in the presence of 12 nM SNAP488–APC-C revealed that APC-C bound the whole length of the microtubule wall and accumulated at the ends of depolymerising microtubules (Fig. 1D). The fluorescence intensity increased consistently as the depolymerisation time progressed, becoming more intense close to the seeds (Fig. 1E). In contrast, in line with our previous observation (Serre et al., 2019), APC-C did not accumulate at the ends of polymerising microtubules (Fig. 1D). APC-C can therefore accumulate autonomously at the ends of depolymerising microtubules.

### The C-terminal domain of APC forms ring-like tubulin oligomers around microtubules

Having observed APC-C to bind all along the microtubule wall (Fig. 1D), we next used electron microscopy to investigate the structure of the APC-C–microtubule complex. Cryo-electron microscopy images revealed that APC-C bundled microtubules and could also organise free tubulin, leading to the formation of tubulin rings with a diameter of 33–38 nm (Fig. S2A,B), similar to the diameter of the tubulin rings that form spontaneously in solution (Arnal et al., 2004; Shemesh et al., 2018). Strikingly, in the presence of both free tubulin and microtubules, APC-C induced an unusual microtubule decoration consisting of ring-like tubulin oligomers wrapped around taxol- or GMPCPP-stabilised microtubules (Fig. 2A; Fig. S2C,D). Ni-NTA gold particles specifically targeting 6× histidine-labelled APC-C revealed the presence of APC-C along the microtubules decorated with rings of tubulin (Fig. S2E). From cryo-electron microscopy images and using single-particle image analysis methods, we calculated a three-dimensional (3D) model of a 13-protofilament (13-pf) microtubule decorated with ring-like tubulin oligomers, measuring about 45 nm in diameter (Fig. 2B). The average axial periodicity of the ring-like tubulin structure was about 10 nm, further suggesting that the ring-like tubulin decoration did not follow the 8-nm periodicity of the tubulin heterodimer in microtubules (Fig. 2C).

### APC-C binds along the protofilament crest

The loose periodicity of the ring-like tubulin structure made it impossible to obtain a high-resolution model (Fig. 2B,C) or to locate the electron density of APC-C on the outer ring-like tubulin structures. Indeed, the ring-like tubulin structures and APC-C density were poorly resolved compared to the central microtubule. This poor resolution is most likely due to the flexibility of the ring structure and the heterogenous binding mode of APC-C.

In contrast, an additional density in the difference map [obtained either by subtracting the signal from a 15-Å low-pass filtered synthetic map of a 13-pf microtubule (Cook et al., 2020) from the original cryo-electron map or by subtracting the signal calculated from the refined atomic model of the 13-pf microtubule from the original cryo-electron map] was present on the external surface of each microtubule protofilament (Fig. 2D,E). This density could accommodate an extended peptide measuring about 65 Å and spanning the microtubule surface in the vicinity of the H11 and H12 helices of tubulin (Fig. 2E). However, the resolution of our model was too low to clearly distinguish between α- and β-tubulin and to conclude whether APC interacts at the intra- and/or inter-dimer tubulin interface. The extended extra density that we assigned to APC-C is reminiscent of that of tau protein, which also binds along the crest of protofilaments, as shown by the superposition of the

**Table 1. Effects of APC-C and APC-ANS1 on microtubule dynamic parameters**

| | MTs | Growth rate±s.d. (µm/min) | *n* | Time (min) | Shrinkage rate±s.d. (µm/min) | *n* | Time (min) | Frequency of catastrophes±s.d. (event/min) | *n* | Frequency of rescues ($min^{-1}$) | *n* |
|---|---|---|---|---|---|---|---|---|---|---|---|
| **Plus end** | | | | | | | | | | | |
| Tubulin | 43 | 0.91±0.16 | 208 | 1595 | 23.93±9.3 | 164 | 63 | 0.12±0.10 | 180 | 0.11 | 7 |
| APC-C | 55 | 1.74±0.31 | 270 | 2231 | 34.09±15.9 | 197 | 99 | 0.10±0.06 | 203 | 0.75 | 75 |
| APC-ANS1 | 46 | 1.61±0.31 | 197 | 1871 | 34.54±16.9 | 123 | 65 | 0.07±0.03 | 124 | 0.55 | 36 |
| **Minus end** | | | | | | | | | | | |
| Tubulin | 36 | 0.34±0.10 | 191 | 1101 | 21.77±10.0 | 163 | 13.7 | 0.16±0.05 | 161 | 1.10 | 15 |
| APC-C | 25 | 0.75±0.17 | 172 | 1221 | 41.96±23.0 | 137 | 13.6 | 0.11±0.04 | 143 | 7.35 | 100 |
| APC-ANS1 | 34 | 0.62±0.15 | 200 | 1548 | 44.27±23.0 | 146 | 14.3 | 0.10±0.04 | 172 | 6.85 | 98 |

*n*, number of events; s.d., standard deviation; MTs, microtubules.

Journal of Cell Science (2022) 136, jcs260152. doi:10.1242/jcs.260152

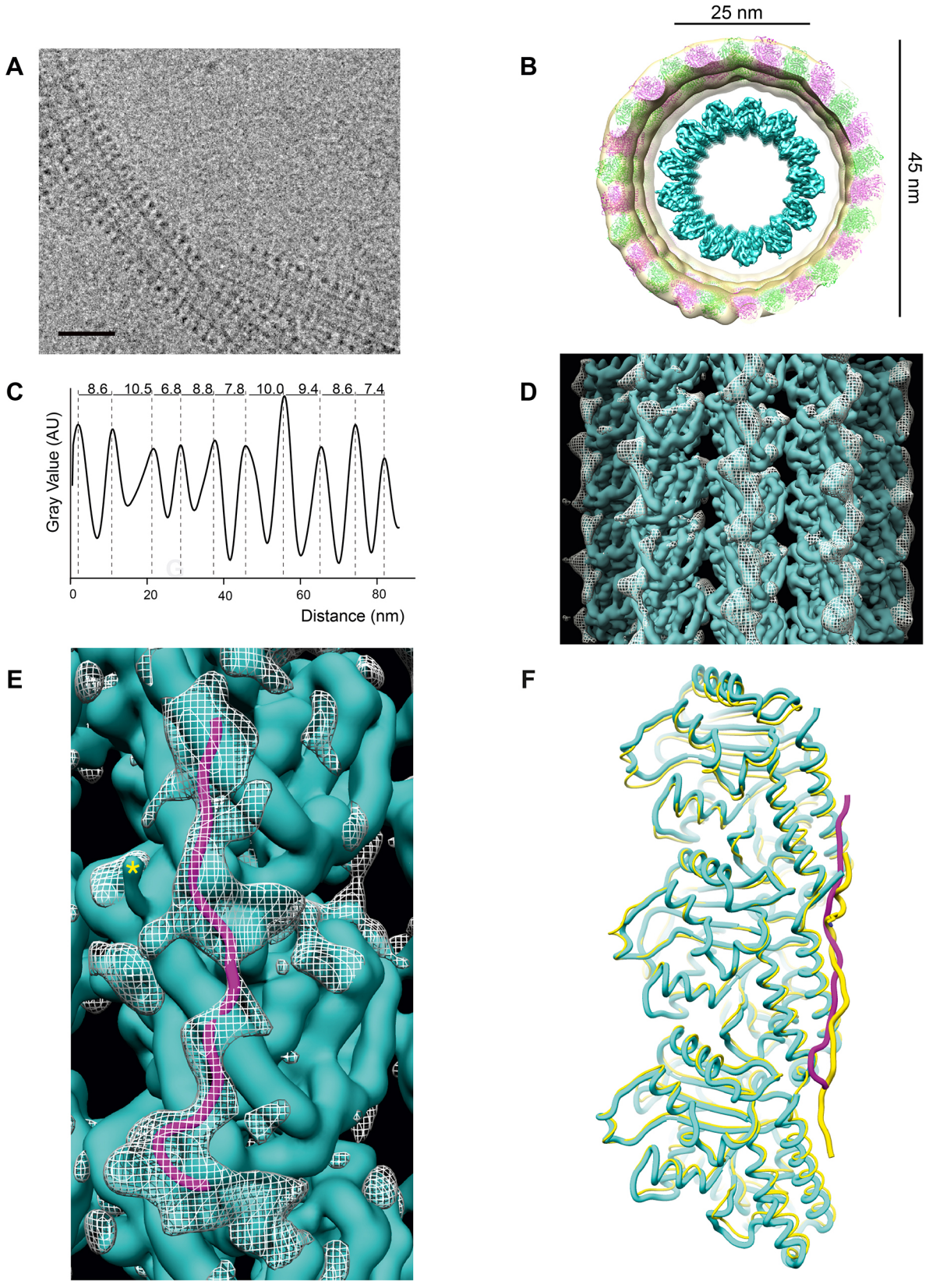


**Fig. 2.** See next page for legend.

atomic model of tau's R2 tubulin binding motif with APC-C C-α chain (Fig. 2F) (Kellogg et al., 2018). By analogy with the structural data provided in studies of kinesin-13 and tau (Benoit et al., 2018; Kellogg et al., 2018), we propose that APC-C interacts with similar sites on the curved tubulin oligomers constituting the outer ring-like tubulin structure.

**Fig. 2. The C-terminal domain of APC forms ring-like tubulin structures around microtubules.** (A) Cryo-electron microscopy image showing examples of taxol-stabilised microtubules decorated by ring-like tubulin structures in the presence of APC-C. Scale bar: 50 nm. (B) 3D electron microscopy reconstruction of one microtubule segment (cyan) decorated with ring-like tubulin oligomers (pale yellow). Atomic models of the tubulin heterodimer (green and pink; PDB ID: 6B0C; Benoit et al., 2018) were fitted inside the cryo-electron microscopy model of the ring-like tubulin structure. (C) An example of the periodicity of tubulin–APC-C decoration around taxol-microtubules. AU, arbitrary units. (D) Difference map between a 15-Å low-pass-filtered synthetic map of a 13-pf microtubule (white mesh) (Cook et al., 2020) and the original cryo-electron map (cyan). (E) Model of the APC-C C-α chain (in magenta) fitted to the residual density of the difference map (white mesh) between the refined atomic model and original cryo-electron map (cyan). (F) Orthogonal view along the axis of one protofilament. The APC-C C-α chain is shown in magenta. The atomic model of tau bound to the microtubule surface (PDB code: 6CVN) fitted within the initial APC cryo-electron microscopy map is shown in yellow. ~~The C-terminus of tubulin is marked by a star~~. The tau–tubulin structure was superposed with the refined atomic model of tubulin (cyan) within the initial APC-C–microtubule map.

AQ20: AQ20

## APC-C exhibits at least two distinct tubulin-binding domains

Decoration of microtubules by ring-like tubulin oligomers requires a minimum of two distinct tubulin-binding sites: one bound to the microtubule lattice and the other to the ring-like tubulin structure. This type of binding could result from APC-C dimerisation or from the presence of multiple tubulin-binding sites within the APC-C sequence. To determine which structure was involved, we used the APC-ANS1 fragment, which behaves like APC-C with respect to microtubule dynamics (Table 1), but is clearly monomeric in solution (Fig. S3A,B). Cryo-electron microscopy images revealed that APC-ANS1 can also decorate microtubules with ring-like tubulin oligomers (Fig. S3C), displaying a similar pattern to that of APC-C. Therefore, each APC-ANS1 monomer contains a minimum of two distinct sites interacting with the tubulin heterodimers present either in the outer ring-like structure or incorporated within the microtubule wall.

To more precisely define these different APC tubulin-binding domains, we designed three overlapping peptides (F1, F2 and F3) within the basic domain of APC-ANS1 (Fig. S3D). Each of these peptides could bind microtubules and form oligomeric tubulin rings in solution (Fig. S3E,F). However, apart from a few rare decorations observed with the F3 fragment, none decorated microtubules with ring-like tubulin oligomers to the same extent as APC-C (Fig. S3F). Based on these results, we delimited two non-overlapping regions required for microtubule interaction: TBS1 (residues 2201–2302) and TBS2 (residues 2311–2365) (Fig. 3A).

To further investigate the regions required for microtubule binding, all the arginine and lysine residues present in TBS1 or TBS2 were mutated to alanine to abolish electrostatic interactions with the negative surface of tubulin dimers. We then investigated whether APC-C-TBS1 (i.e. mutated in the TBS2 site) and APC-C-TBS2 (i.e. mutated in the TBS1 site) could induce the formation of ring-like structures around microtubules in the presence of soluble tubulin. As expected, and unlike APC-C, microtubules decorated with rings were not observed in the presence of either APC-C-TBS1 or APC-C-TBS2 (Fig. 3B). To confirm this result, we also compared the ability of green-fluorescent mutated and wild-type forms of APC-ANS1 to bind microtubules and decorate them with red-fluorescent soluble tubulin. Loss of one of the two TBS sites did not abolish the interaction of APC-ANS1 with microtubules (Fig. 3C; Fig. S4A,B) but prevented the recruitment of free tubulin to microtubules (Fig. 3D) and decreased the effect of APC-ANS1 on microtubule growth and shrinkage rates (Fig. S1; Table S1).

These results indicate that APC-C contains at least two adjacent tubulin-binding sites presenting similar properties in terms of tubulin and microtubule binding (Fig. 3). Both sites are required for decoration of microtubules with ring-like tubulin oligomers and for APC-C to regulate microtubule dynamics.

The 3D models of TBS1 and TBS2 predicted by the Robetta/RosettaFold server (Baek et al., 2021) were superposed on the R2 tubulin-binding domain of tau within the additional density defined above (Fig. S4C). Interestingly, this modelling highlighted two superposable clusters of basic amino acids involved in the interaction with microtubules (Fig. S4D,E), suggesting that these two structural microtubule-associated-proteins (MAPs) share a common microtubule-binding mode.

For subsequent cellular studies, we used APC-C-TBS1 (mutated in the TBS2 site) as mutation of the TBS1-binding site reduced microtubule binding compared to the wild-type form (Fig. S4B).

## APC-C is located on spindle microtubules and in the vicinity of kinetochores during metaphase

Ring-like structures have been proposed to play a role in coupling chromosome movement and microtubule dynamics during mitosis (Cheeseman and Desai, 2008; Davis and Wordeman, 2007). Having observed that APC-C modulates microtubule dynamics and also induces the formation of ring-like tubulin structures around microtubules *in vitro*, we next examined its location during mitosis in RPE-1 cells expressing APC-C (Fig. 4).

In these experiments, APC-C mainly localised to the centrosomes and spindle microtubules (either kinetochore or interpolar microtubules, which were indistinguishable at the resolution available) (Fig. 4A,B). APC-C also partially colocalised with CENP-E, a component of the outer kinetochore involved in chromosome congression (Kapoor et al., 2006) (Fig. 4C,D). This colocalisation was greatly reduced following treatment with nocodazole, which causes complete depolymerisation of spindle microtubules (Fig. 4C,D), indicating that the positioning of APC-C at the outer kinetochores is microtubule dependent. Similar localisation results were obtained with the mutant APC-C-TBS1 (Fig. 4). Based on these observations, APC might be involved at the kinetochore–microtubule interface, as previously suggested (Banks and Heald, 2004; Draviam et al., 2006; Fodde et al., 2001b; Kaplan et al., 2001).

AQ5: AQ5

## Wild-type but not mutant APC-C partially rescues chromosome congression defects during metaphase

From its localisation in cells and its *in vitro* properties, we postulated that APC-C might link microtubule dynamics to chromosome movements during metaphase and anaphase. To test this hypothesis, we depleted RPE-1 and HeLa cells of endogenous APC with a specific siRNA (Fig. S5). In agreement with previous studies (Bakhoum et al., 2009; Draviam et al., 2006; Green et al., 2005), APC knockdown cells displayed a drastic increase in the percentages of metaphase cells exhibiting misaligned chromosomes and anaphase cells with lagging chromosomes (Fig. 5A–F). Expression of APC-C, but not the APC-C-TBS1 mutant, rescued the metaphase chromosome misalignment in these cells (Fig. 5C,E). Interestingly, complementation with APC-C poorly rescued chromosome segregation defects during anaphase (Fig. 5D,F).

We next wondered whether the expression of APC-C could also complement the function of APC in human colorectal tumour SW480 cells, which express a truncated form of APC encompassing the N-terminal third of the protein (up to residue 1338) and lacking the whole APC-C domain. SW480 cells exhibited a relatively high

Journal of Cell Science (2022) 136, jcs260152. doi:10.1242/jcs.260152

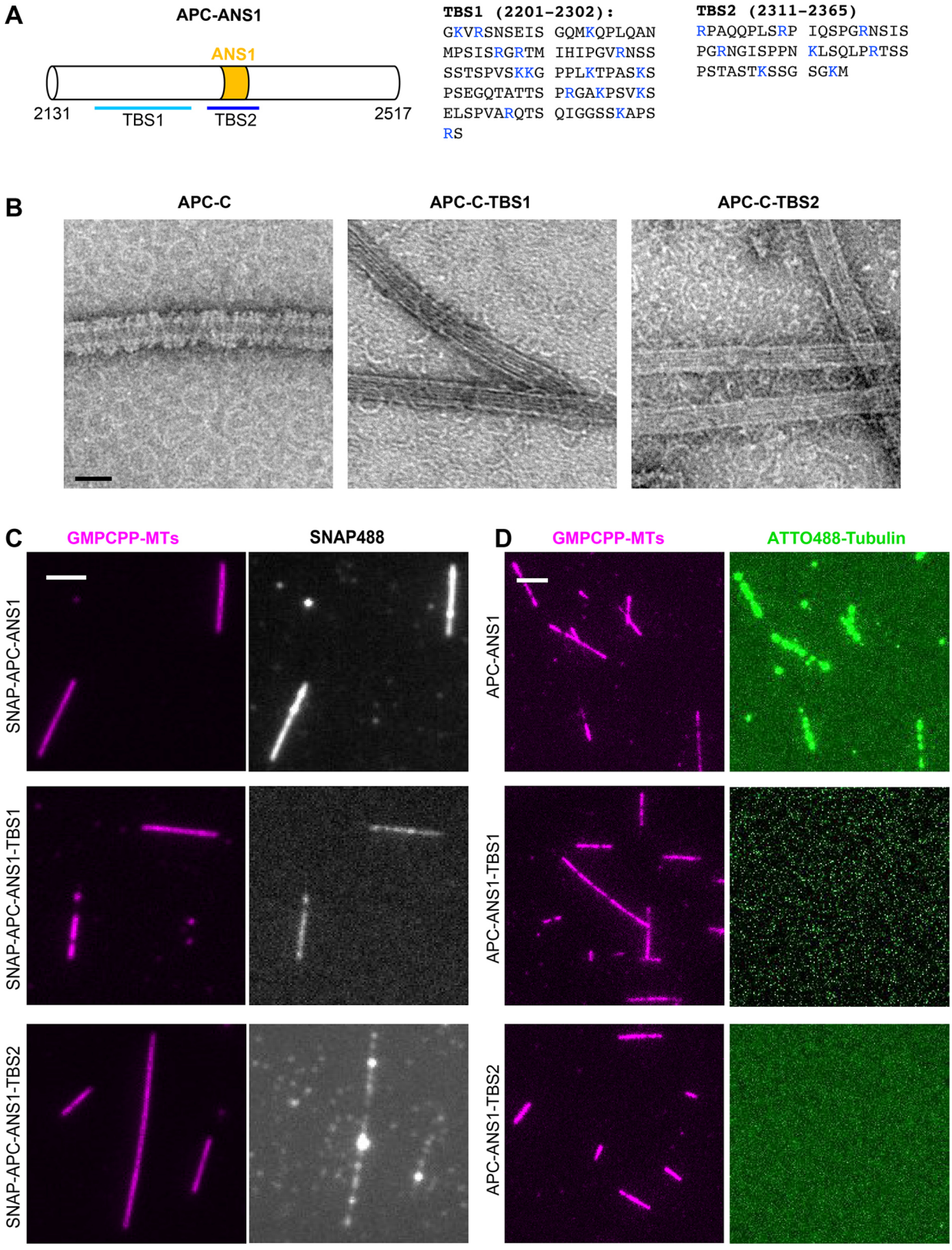


**Fig. 3. Decoration of microtubules by tubulin oligomers requires the full basic domain of APC.** (A) Location of the TBS1 and TBS2 tubulin-binding sites within the APC-ANS1 sequence and their amino acid sequences. The basic residues that were mutated to alanine are shown in blue. (B) Negative-staining electron microscopy images of taxol-stabilised microtubules incubated with free tubulin and APC-C or APC-C mutated for the basic domain (APC-C-TBS1 and APC-C-TBS2). Scale bar: 50 nm. (C) TIRF images of Atto561-GMPCPP-microtubules (magenta) incubated with 100 nM fluorescent SNAP488–APC-ANS1, SNAP-488–APC-ANS1-TBS1 or SNAP488–APC-ANS1-TBS2 (grey). (D) TIRF images of Atto561-GMPCPP-microtubules (magenta) incubated with 5 µM Atto488–tubulin (green) and 100 nM APC-ANS1, APC-ANS1-TBS1 or APC-ANS1-TBS2. Scale bars: 2 µm. ~~Images are representative of xxxxx experiments.~~

AQ21: AQ21

Journal of Cell Science (2022) 136, jcs260152. doi:10.1242/jcs.260152

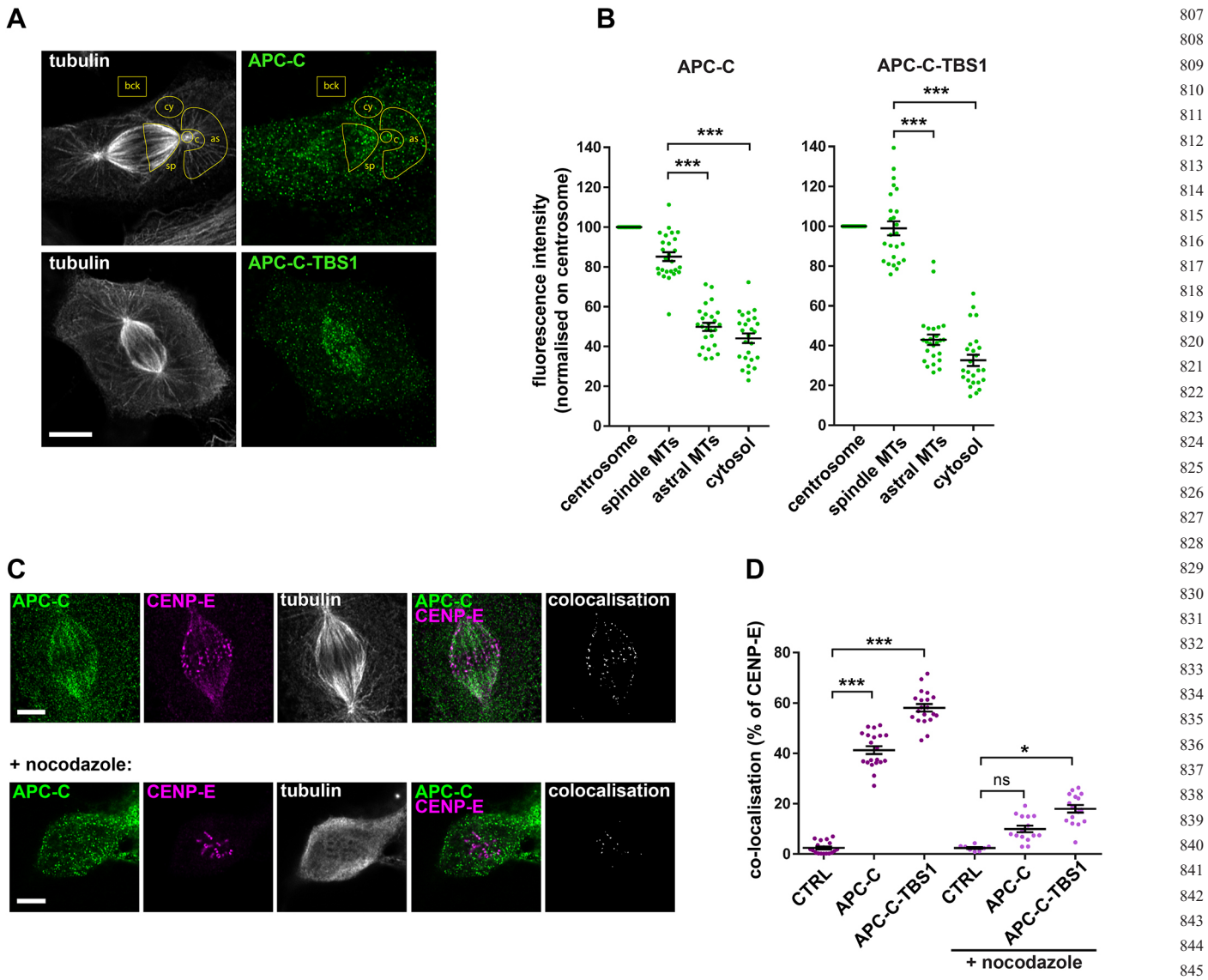


**Fig. 4. APC-C and APC-C-TBS1 mainly localise on centrosomes, spindle microtubules and at the microtubule–kinetochore interface.** (A) Representative Airyscan images (one focal plane) of metaphase RPE-1 cells expressing EGFP–APC-C or EGFP–APC-C-TSB1 (green) and labelled for tubulin (grey). The fluorescence intensity of EGFP constructs was measured in the delimited ROIs (an example of ROI is shown for one hemi-spindle; 'bck, background; c, centrosome; sp, spindle microtubules; as, astral microtubules; cy, cytosol). Scale bar: 5 µm. (B) Fluorescence intensity of APC-C and APC-C-TBS1 on spindle microtubules, astral microtubules and in the cytosol (intensities normalised relative to the signal for the centrosome). MTs, microtubules. Data are expressed as mean±s.e.m. A total of 25 cells from three independent experiments were quantified. ***$P$<0.001 (Kruskal–Wallis test with Dunn's multiple comparisons). (C) Representative Airyscan images of metaphase RPE-1 cells transfected with EGFP–APC-C (green) and labelled for CENP-E (magenta) and tubulin (grey), in the absence (upper panels) or presence (lower panels) of nocodazole. Scale bar: 5 µm. The right-most panels (colocalisation) correspond to binary images showing the overlap of EGFP–APC-C on CENP-E after segmentation in the two channels (see Materials and Methods). (D) The percentage of colocalisation between EGFP–APC-C or EGP–APC-C-TBS1 and CENP-E in the absence and presence of nocodazole, compared to mock-transfected cells (CTRL). Data are expressed as mean±s.e.m. The total number of cells analysed (from left to right) were 18, 20, 20, 8, 15 and 16, from two experiments. ns, not significant; *$P$<0.05; ***$P$<0.001 (Kruskal–Wallis test with Dunn's multiple comparisons).

percentage of defects during metaphase and anaphase (Fig. 5G,H). As above, expression of APC-C reduced the percentage of metaphase chromosome misalignment (Fig. 5G) but had no impact on chromosome segregation defects during anaphase (Fig. 5H). As expected, the APC-C-TBS1 mutant provided no complementation for either the metaphase or anaphase defects (Fig. 5G,H).

To further analyse the role played by APC-C in mitosis, we examined the duration of mitosis using time-lapse experiments (Fig. 6A). APC depletion in RPE-1 cells resulted in a mitotic delay, with a lengthening of the duration between nuclear envelope breakdown (NEB) and metaphase chromosome alignment (Fig. 6B). In agreement with the results described above (Fig. 5), this delay was rescued, with the durations returning to close to those recorded for control cells, upon expression of APC-C. Once again, expression of APC-C-TBS1 failed to rescue the defects (Fig. 6B). In contrast, APC depletion had no effect on the duration between metaphase chromosome alignment and the onset of anaphase (Fig. 6C).

Overall, these results indicate that APC-C contributes to regulating chromosome congression during metaphase through processes involving its multiple tubulin-binding sites.

Journal of Cell Science (2022) 136, jcs260152. doi:10.1242/jcs.260152

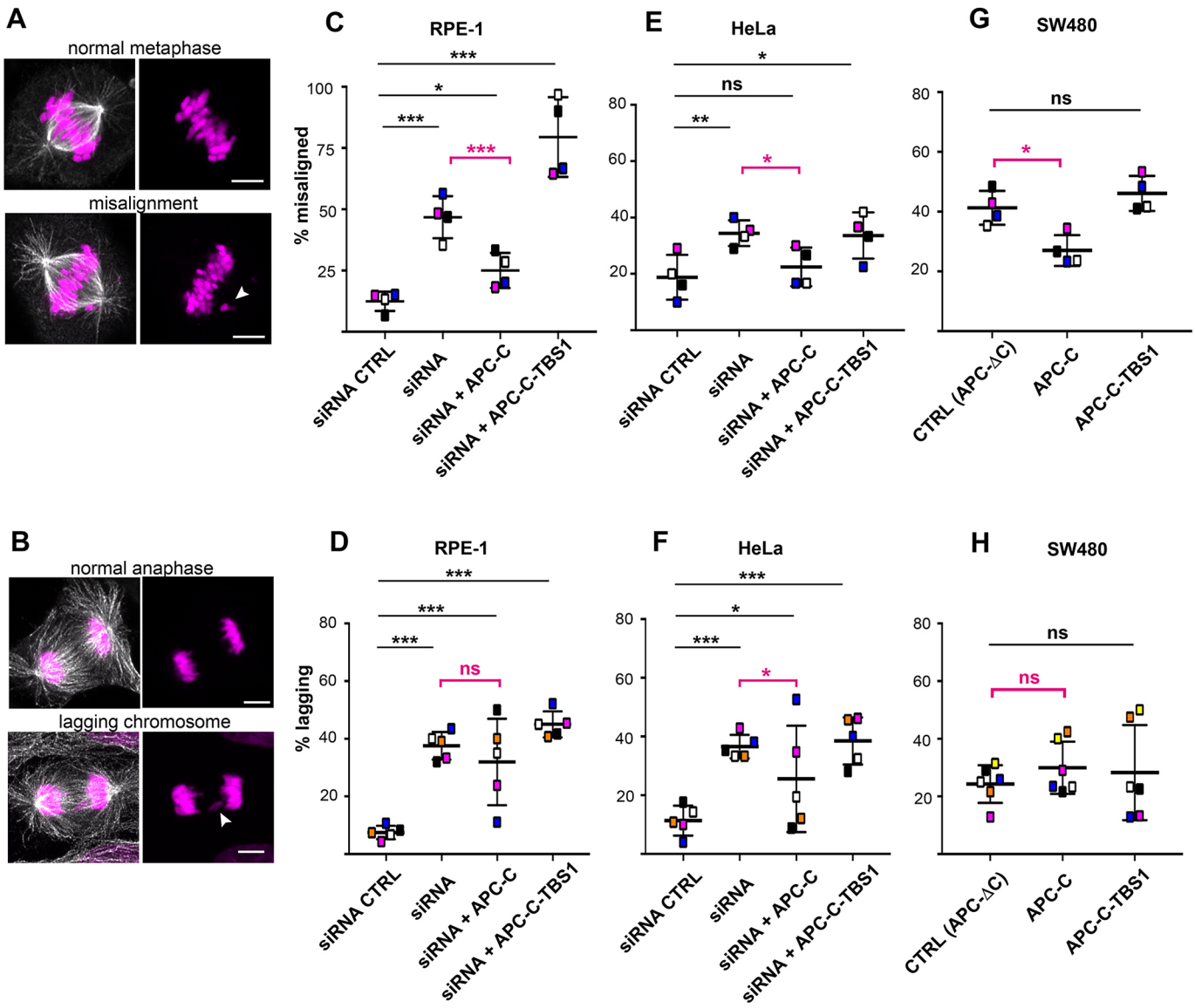


**Fig. 5. APC-C can rescue chromosome misalignment during metaphase.** (A) Representative images of RPE-1 cells showing normal metaphase or abnormal metaphase with misaligned chromosomes (arrowhead). (B) Representative images of RPE-1 cells showing normal anaphase or abnormal anaphase with lagging chromosomes (arrowhead). Cells were labelled for tubulin (grey) and DNA (magenta). Scale bars: 5 µm. (C–H) Percentages of cells exhibiting misaligned chromosomes or exhibiting lagging chromosomes. RPE-1 (C,D) and HeLa (E,F) cells were transfected with control siRNA (siRNA CTRL), siRNA against APC (siRNA), siRNA+APC-C construct and siRNA+APC-C-TBS1 construct. SW480 cells (G,H) were transfected with APC-C or APC-C-TBS1 constructs. Total number of metaphase cells analysed: RPE-1, *n*=121–133; HeLa, *n*=120–122; SW480, *n*=147–161 (data correspond to the mean from four independent experiments). Total number of anaphase cells analysed: RPE-1, *n*=110–144; HeLa, *n*=142–160; SW480, *n*=186–197 (data represent the mean from four to six independent experiments). To determine statistical significance, normal and abnormal cells were distributed in contingency tables and analysed by applying Fisher's exact test. ns, not significant; **P*<0.05; ***P*<0.01; ****P*<0.001. The colour code corresponds to the different experiment replicates.

## DISCUSSION

This study aimed to elucidate the intrinsic properties of the C-terminal domain of APC (APC-C), in which the main cytoskeleton-interacting sites are located – sites that are absent from the pathological forms. Our results revealed new properties of APC with regard to its interaction with microtubules and tubulin, and to its role during mitosis.

APC is a large scaffold protein and its interaction network includes partners involved in a wide range of cellular processes (Nelson and Näthke, 2013; Rusan and Peifer, 2008). APC was primarily identified as a microtubule stabiliser, and its C-terminal domain was ascribed a major role in microtubule interaction (Zumbrunn et al., 2001). In our model derived from cryo-electron microscopy data, APC-C, the domain that encompasses the microtubule-binding sites, could adopt an extended conformation spanning the protofilament crest at the interface between tubulin monomer and/or dimers. This model is reminiscent of the interaction described between neuronal tau and microtubules (Kellogg et al., 2018), and corroborates results of an early study that highlighted analogies between APC and tau (Deka et al., 1998) with regard to tubulin assembly and microtubule bundling. Interestingly, this mode of microtubule binding has also been described at a low resolution for MAP2 (Al-Bassam et al., 2002), another structural MAP present in neurons. It could therefore

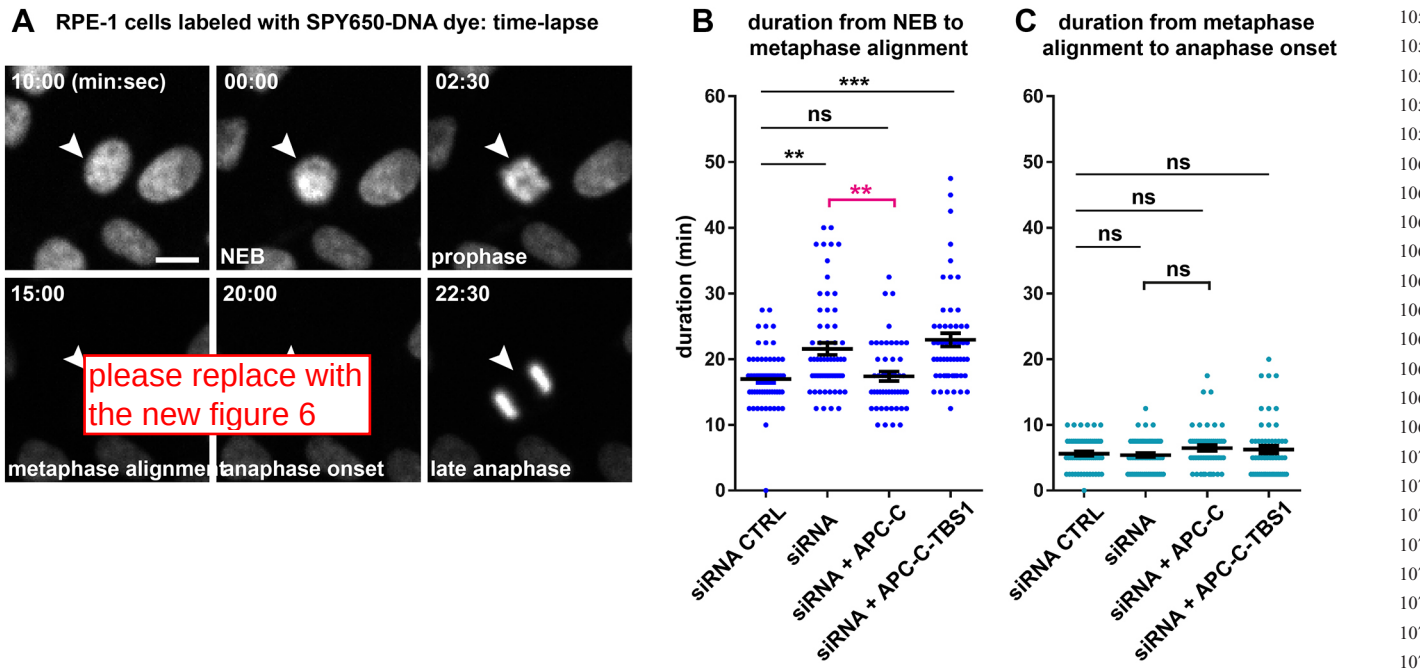


**Fig. 6. Time between NEB and metaphase alignment is prolonged in APC-depleted cells but can be restored in the presence of APC-C.** (A) Sequence of images of RPE-1 cells at the indicated times (in min:s) relative to NEB. Arrowheads point towards a dividing cell. Scale bar: 10 µm. (B,C) Plots showing the time from NEB to metaphase alignment (B) and from metaphase alignment to anaphase onset (C) in RPE-1 cells transfected with control siRNA (siRNA CTRL), siRNA against APC (siRNA), siRNA+APC-C construct and siRNA+APC-C-TBS1 construct. Points represent individual durations and data are expressed as mean±s.e.m. Total number of mitotic cells analysed: *n*=56, 64, 51, 55, respectively, from four different movies in each condition. ns, not significant; ***P*<0.01; ****P*<0.001 (Kruskal–Wallis test with Dunn's multiple comparisons).

AQ22

AQ22:

AQ23

AQ23:

constitute a hallmark of this family of MAPs exhibiting basic intrinsically disordered microtubule-binding sites. Despite its analogies with structural MAPs that promote microtubule assembly, APC exhibits unique properties. Indeed, besides increasing microtubule assembly, the APC-C domain also promotes the disassembly of tubulin at both ends of microtubules, behaving as a depolymerase (Fig. 1B; Table 1). Very few proteins exhibit this type of antagonistic activity. To our knowledge, only the plus-end-tracking protein XMAP215, which is mainly described as an efficient tubulin polymerase, has also been identified as a microtubule-depolymerising factor under specific conditions (Brouhard et al., 2008). However, whereas the activity of XMAP215 seems restricted to the microtubule plus ends, APC-C promotes microtubule dynamics at both ends (Table 1).

Thus, APC could regulate microtubule dynamics across a large panel of processes, including assembly of the mitotic spindle and organisation of acentrosomal microtubule arrays in neurons and epithelial cells (Akhmanova and Hoogenraad, 2015; Weaver and Walczak, 2015). The location of APC at the kinetochore–microtubule interface is consistent with its role in mitosis, during which it could tune the alternating growing and shortening phases through its activity at microtubule ends. In dividing cells, during metaphase, microtubules repeatedly shrink and grow until all the chromosomes are aligned on the metaphase plate and correctly attached to spindle microtubules; during anaphase, microtubule-depolymerising forces predominate to pull the chromosomes towards the poles of the cell. The hypothesis that APC is involved in these processes also explains the chromosome misalignment and mis-segregation observed in APC knockdown cells and in SW480 cancer cells (Fig. 5). Complementation with the C-terminal domain of APC restores metaphase chromosome alignment and normal metaphase duration, but does not fully restore the defects relating to lagging chromosomes in anaphase (Fig. 5). Accordingly, the fact that APC-C stimulates microtubule dynamics by increasing microtubule growth and shrinkage rates and by stimulating the rescue frequency might better correspond to the microtubule behaviour required during metaphase to achieve chromosome congression, rather than the behaviour required during anaphase.

In addition to the effects of APC on regulating microtubule dynamics, our results highlight a novel and intriguing property related to its tubulin-binding capacity. Using electron microscopy, we observed that APC fragments containing the microtubule-binding domain (i.e. APC-C and its shorter form APC-ANS1) organised ring-like structures composed of tubulin around microtubules (Fig. 2). Similar tubulin structures around microtubules have been observed by electron microscopy for the microtubule-binding domains of kinesin-13 and Ska-1, both of which are located at the kinetochores during mitosis (Benoit et al., 2018; Monda et al., 2017). Based on this similarity, we hypothesised that these peculiar ring-like structures correspond to functional features shared by kinesin-13, Ska-1 and APC. By analogy with the Dam-1/DASH complex, an essential component of the yeast kinetochores that self-organises as rings around microtubules (Miranda et al., 2005; Westermann et al., 2005; Ramey et al., 2011), it has been suggested that these rings play a key role in linking kinetochore movement to microtubule dynamics during mitosis (Davis and Wordeman, 2007; Cheeseman and Desai, 2008). In particular, these rings were proposed to convert the force generated by microtubule depolymerisation into movement along the lattice, thus allowing the chromosomes to segregate towards the poles during anaphase or to oscillate during metaphase. In this context, the ring-like tubulin structures generated by the microtubule-binding domain of kinesin-13, Ska-1 and now APC could reflect the ability of these three proteins to increase

AQ6:

microtubule shrinkage and link microtubule depolymerisation to chromosome movements during mitosis.

The decoration of microtubules with ring-like tubulin structures results from the presence of two tubulin-binding sites per APC-C monomer, which allow APC to simultaneously bind straight tubulin in the microtubule lattice and bent tubulin in the ring-like tubulin structures (Fig. 3). Mutation of one of these tubulin-binding sites is sufficient to prevent the recruitment of tubulin around the microtubule lattice, and the resulting mutant fails to restore metaphase alignment and chromosome segregation in APC knockdown cells or SW480 cancer cells (Fig. 5). The presence of multiple tubulin-binding sites – required to decorate microtubules with tubulin oligomers *in vitro* – is therefore essential for the mitotic functions of APC. Along this line, molecular models have proposed that for a majority of proteins that track depolymerising microtubule ends, multiple tubulin-binding sites composed of disordered and positively charged sequences, such as the sequence of APC-C, are required to efficiently link microtubule shrinkage to movement of the associated cellular cargoes attached to these proteins (Volkov, 2020). Such models are based on the ability of these protein couplers to remain attached to the microtubule ends as they shorten through their multiple tubulin-binding domains. We hypothesise that curved tubulin structures released from depolymerising microtubules might be pulled by APC-C as it diffuses along the microtubule wall (Baumann et al., 2020). Such a mechanism would enhance breaking of the lateral contacts of the protofilament and explain how APC-C accelerates the microtubule shrinkage rate. Accordingly, the APC-C mutant incompetent to decorate microtubules with tubulin oligomers exhibits a reduced microtubule-depolymerising activity.

Finally, the existence of multiple tubulin-binding sites in APC-C might favour microtubule bundling, a function previously attributed to APC both in cells and in cell-free systems (Deka et al., 1998; Kahn et al., 2018; Mogensen et al., 2002; Zumbrunn et al., 2001). In a mitotic context, APC could therefore enhance microtubule bundling at the kinetochore and simultaneously coordinate the overall dynamics of bundled microtubules. Through this activity, it could have an impact on the formation of the metaphase plate.

From its presence at the microtubule–kinetochore interface and the propensity of its microtubule-binding domain to increase microtubule dynamics, in particular, microtubule shrinkage, to bind curved tubulin, to accumulate at microtubule depolymerising ends and to decorate microtubules with tubulin oligomers as described for other kinetochore proteins, we propose that APC is a component of the molecular complexes regulating the coupling of kinetochore movements and microtubule dynamics at least during metaphase. The data presented here provide new molecular evidence contributing to our understanding of the mitotic function of this major regulator of cellular integrity. For more than two decades, cellular studies have highlighted the major role played by APC in preventing cancer development and aneuploidy. Our results confirm a role for APC in normal functions of the mitotic spindle owing to its regulation of microtubule dynamics. We also present molecular evidence of the specific role played by the C-terminal domain of APC, the lack of which is associated with chromosome instability.

## MATERIALS AND METHODS

### Plasmids and siRNAs

To construct pEGFP-APC-C and pEGFP-APC-C-TBS1 plasmids, APC-C and APC-C-TBS1 were PCR amplified from the pET20b (Novagen) constructs described in Serre et al. (2019) and were inserted into the pEGFP-C1 plasmid (xx source xx) using the In-Fusion HD Cloning kit (Clontech) and the primers indicated in Table S2. Plasmid DNA for co transfection was prepared using a Plasmid Endofree Midi Kit (QIAGEN, Hilden, Germany). Additional DNA sequences used in this study are listed in Table S2. siRNAs directed against APC and control siRNA (siRNA CTRL) (Table S2) were purchased from Eurofins.

### Protein preparation

Proteins were purified as described in Serre et al. (2019). Briefly, xxxxxxxxx.

### *In vitro* microtubule dynamics assays

To explore how APC-C influences microtubule dynamics by TIRF microscopy, flow chambers were prepared and perfused with stable fluorescent (ATTO-561) GMPCPP-microtubule seeds, as described previously (Ramirez-Rios et al., 2017). Microtubule nucleation was then induced from seeds by adding the following mixture: 15 µM bovine tubulin containing 15% fluorescent ATTO-488–tubulin in BRB80 buffer (80 mM PIPES, 1 mM EGTA, 1 mM $MgCl_2$, pH 6.8), 100 mM KCl, 3% (v/v) glycerol, 1 mM GTP, 1% (w/v) bovine serum albumin, 0.05% (w/v) methyl cellulose 4000 cp (xx source xx), 4 mM dithiothreitol, 1 mg/ml glucose, 70 mg/ml catalase (xx source xx) and 580 mg/ml glucose oxidase (xx source xx). APC-C or APC-ANS1 (50 nM) were added where indicated. Samples were observed for 45 min (recording one image every 5 s) at 32°C on an inverted microscope (Nikon) equipped with an iLas$^2$ TIRF system (Roper Scientific), a cooled charged-coupled EMCCD camera (Photometrics) and a warm stage controller (Linkam Scientific). The system was controlled using MetaMorph software (Molecular Devices). The parameters of microtubule dynamics were determined from kymographs using ImageJ software (Schneider et al., 2012) and an in-house KymoTool (Ramirez-Rios et al., 2017). Growth and shrinkage rates were obtained from the slopes of the microtubule growth and shrinkage phases, respectively. The catastrophe frequency was calculated by dividing the number of events by the time spent in growing state per microtubule. Due to large variations between microtubules, the rescue frequency was calculated by dividing the total number of events by the total time spent in shrinking state for each condition. The data presented in Table 1 and Table S1 are from two or three independent experiments.

### Design and mutation of tubulin-binding sites

Based on previous studies that highlighted the contribution of APC sequences (residues 2244–2312 and 2326–2371) to interactions with microtubules (Deka et al., 1998; Okada et al., 2010), three overlapping peptides (F1, F2 and F3) were designed within the basic domain of APC-ANS1 (Fig. S3D). These peptides were used to more precisely characterise the role of distinct regions in the decoration of microtubules by ring-like tubulin oligomers using co-sedimentation assays (Fig. S3E) and negative-staining electron microscopy (Fig. S3F). From the results obtained, and by comparing the sequences of the three fragments, two non-overlapping regions TBS1 (residues 2201–2302) and TBS2 (residues 2311–2365) were delimited (Fig. S3D). The arginine and lysine residues present in TBS1 or TBS2 were mutated to alanine (by to a total of 16 and ~~eight~~ mutations in the TBS1 and TBS2 nucleotide sequences, respectively). The mutations were confirmed by sequencing. The resulting mutant sequences were inserted into the APC-C and APC-ANS1 nucleotide sequences to study the effect of a lack of one of the two tubulin-binding sites on microtubule decoration and dynamics.

### Co-sedimentation assay with taxol-stabilised microtubules

To test the microtubule-binding properties of APC-ANS1, APC-ANS1-TBS1, APC-ANS1-TBS2 and the F1, F2 and F3 fragments, 1 µM taxol-stabilised microtubules and 2 µM APC-ANS1, APC-ANS1-TBS1 or APC-ANS1-TBS2, or the F1, F2 or F3 fragments were added to BRB80 buffer supplemented with 50 mM KCl, and incubated for 10 min at 35°C. An aliquot (20 µl) of this mixture was then overlaid on a 40-µl cushion of 60% (w/v) sucrose in BRB80 buffer and 50 mM KCl, and centrifuged at xxxxx ***g*** (Beckman Coulter rotor TLA-100) for 45 min at 35°C. The protein

AQ7 AQ8 AQ9: AQ10:

content of the supernatant and pellet were analysed by migration on 4–15% gels by SDS-PAGE revealed by Coomassie Blue staining. Bands corresponding to APC-ANS1 and its fragments were quantified using ImageJ (Schneider et al., 2012).

### Negative-staining electron microscopy

2 µM taxol-stabilised microtubules, 5 µM APC-C, 5 µM bovine brain tubulin in BRB80 buffer and 50 mM KCl were mixed together. An aliquot of this solution (4 µl) was loaded onto a glow-discharged carbon-coated grid (xx source xx). After incubation for 30 s, the grid was blotted (Whatman Paper N°4, xx source xx) and placed upside down in contact with a drop of 1 nM Ni-NTA-Nanogold (5-nm diameter, Nanoprobes), BRB80 buffer and 50 mM KCl for 4 min at room temperature. The grid was then washed with BRB80 buffer ~~and~~ 50 mM KCl, and stained with 2% (w/v) uranyl acetate for 30 s. APC-C with and without 6× histidine tags were tested in parallel. Grids were observed using an FEI Tecnai F20 200 kV electron microscope equipped with a 4K×4K FEI Ceta CMOS camera (FEI Company). Images were taken in low-dose mode.

For other negative-staining microscopy experiments, 4 µl of protein solution were loaded onto glow-discharged carbon-coated grids. After incubation for 30 s, grids were blotted and stained with 2% (w/v) uranyl acetate.

### Cryo-electron microscopy

Taxol-stabilised microtubules and GMPCPP microtubules were prepared from bovine tubulin. Taxol-stabilised microtubules (2 µM) were mixed with 5 µM APC-C or APC-ANS1 and 5 µM tubulin in BRB80 buffer with 50 mM KCl. An aliquot of this mixture (4 µl) was deposited on a glow-discharged Quantifoil R2/2 300 mesh carbon/copper grid mounted on a grid plunger (Vitrobot IV, Thermo Fisher Scientific). Grids were blotted for 1 s at 32°C with 100% humidity, flash frozen in liquid ethane and stored in liquid nitrogen until imaging. Images were acquired at 200 kV on a Glacios electron microscope (Thermo Fisher Scientific) equipped with a Falcon-II direct electron detector. Data acquisition was performed using EPU software (Thermo Fisher Scientific). Images were acquired at 73,000× magnification, pixel size 1.96 Å at the specimen level, 40 electrons/Å$^2$/movie, 1.5 s exposure time and 29 frames per movie; the defocus ranged from −3.0 to −1.5 µm (Fig. S6).

Movie frames (~~2–28~~) were aligned using MotionCor2 (Zheng et al., 2017) and the corresponding contrast transfer function (CTF) parameters were estimated with CTFFIND4.1 (Rohou and Grigorieff, 2015) on the drift-corrected average. Particles were manually selected using the RELION-3.08 pick start-end coordinates helices option (Scheres, 2015). 320×320 pixel$^2$ helical segments were extracted based on an 82-Å rise. To determine and select the microtubule symmetry, averaged particles were generated (Cook et al., 2020) and a 3D-classification was performed by comparison to reference microtubules (12, 13, 14 and 15 pf). After identification of the most probable symmetry for each microtubule, 14,170 segments corresponding to 13-pf microtubules were selected. Particles were aligned by several steps of auto-refinement (Refine3D, RELION) to determine $\psi$, $\theta$ and $\phi$ angles and *xy* displacements, as well as the most probable seam position for each microtubule (Cook et al., 2020). The 13-fold-helical symmetry was imposed in the last step of refinement with local searches of the helical twist and rise (twist=−27.68°, rise=9.54 Å). Power spectra generated from two-dimensional (2D)-classes of the decorated particles revealed a blurry layer line, around 1/10 nm, in addition to the diffraction layer line at 1/4 nm corresponding to the tubulin monomer. This additional line suggested that the decoration only loosely follows the periodicity of the tubulin dimer. Therefore, the microtubule and outer curved tubulin oligomers were separately refined (Fig. S7). ~~Fig. S6~~ The local-filtered map (LAFTER, CCPEM; Ramlaul et al., 2019) was used to construct a 13-pf microtubule from the tubulin heterodimer (PDB ID 6B0C; Benoit et al., 2018) with Chimera (Pettersen et al., 2004). This model was then refined with REFMAC5, CCPEM (Nicholls et al., 2018)). A difference map was calculated by subtracting the signal calculated from the refined atomic model from the LAFTER cryo-electron map (TEMPy:DifferenceMap, CCPEM; Joseph et al., 2020). A C-α peptide was manually built inside this residual density map using COOT (Emsley et al., 2010). Both the TBS1 and TBS2 sequences were submitted to the Robetta/RosettaFold server (Baek et al., 2021) and the predicted models fitted inside the residual density map using Chimera (Pettersen et al., 2004).

To reconstruct the external tubulin ring, we selected particles exhibiting a regular decoration by a 2D classification and then performed 3D classification using synthetic references of the external ring built from PDB models (based on the PDB structure 6B0C; Benoit et al., 2018) with an axial periodicity of 8 nm or 10 nm. We selected the particles leading to the best map (5928 particles) and aligned them using Refine3D applying the helical symmetry (twist=−27.676° and rise=9.61 Å). The resolution was estimated to 5.3 Å for the microtubule and 25 Å for the outer curved tubulin oligomers (Fourier shell correlation=0.143) (Fig. S6) using a solvent mask.

### Cell culture, transfection and treatment

HeLa and SW480 cells were purchased from CLS Cell Lines (Germany) and hTERT-RPE-1 cells were from LGC-ATCC (France). All cells were free of mycoplasma and were cultured in Dulbecco's modified Eagle medium (DMEM; xx source xx), 4.5 g/l glucose with 10% foetal bovine serum (xx source xx). Transient transfections were carried out with 100 pmol siRNA and/or 1 µg of plasmid DNA per 35-mm dish, using the JetPrime reagent (Ozyme) for HeLa and SW480 cells, or Lipofectamine 3000 reagent (Thermo Fisher Scientific) for RPE-1 cells. HeLa and RPE-1 cells were first transfected with siRNA for 8–24 h and then with plasmid DNA for a further 16–24 h. SW480 cells were only transfected with plasmid DNA for 24 h. To depolymerise spindle microtubules in mitotic cells, cells were treated for 2 h with 20 µM nocodazole (Sigma-Aldrich) at 37°C before fixation.

### Immunofluorescence and image acquisition

For immunofluorescence analysis, cells were fixed by incubation in −20°C methanol for 10 min. The primary antibodies used were: rabbit polyclonal anti-EGFP (x:xxxx, AB3080, Millipore), mouse monoclonal anti-CENP-E (x:xxxx, ab5093, Abcam), rat monoclonal anti-tyrosinated α-tubulin (x:xxxx, clone YL1/2, xx cat. no. xx, xx source xx; Wehland and Willingham, 1983) and mouse monoclonal anti-α-tubulin (x:xxxx, α3-a1, xx cat. no. xx, xx source xx; Peris et al., 2006). Secondary antibodies were coupled to Alexa Fluor 488, Alexa Fluor 647 or Cyanine3 (Jackson ImmunoResearch Laboratories). Standard immunofluorescence procedures were applied. DNA was stained with bisbenzimide Hoechst 33258 (5 µg/ml, Sigma-Aldrich). Images were acquired on a Zeiss LSM 710 confocal microscope equipped with a Zeiss Airyscan module, using a 63× oil-immersion NA 1.4 objective and Zen software (Carl Zeiss MicroImaging).

### Time-lapse experiments

For time-lapse experiments, cells were grown in medium without Phenol Red [Fluorobrite-DMEM (Thermo Fisher Scientific) complemented with 10% foetal bovine serum and 1× GlutaMAX (Thermo Fisher Scientific)] and seeded in ibi-Treat glass-bottomed 35-mm dishes with four-well inserts (80466, ~~BioValley~~). Each well was transfected according to one condition (siRNA CTRL, siRNA, siRNA+APC-C and siRNA+APC-C-TBS1) to allow the four conditions to be filmed in parallel in the same experiment. Approximately 1–2 h before time-lapse capture, RPE-1 cells were incubated in medium containing 1× SPY650-DNA (SC501, Spirochrome, Switzerland) prepared according to the manufacturer's instructions. Cells were then imaged using a 20× NA 0.8 objective on a spinning-disc AxioObserver Z1 microscope (Zeiss/Roper) in a humidified and thermo-regulated chamber. MetaMorph 7.8.5 software (Molecular Devices) was used to perform multi-positioning time-lapse capture in the four wells. In each position, *z*-series images (6-µm range around focus) were taken every 2.5 min with the CSU642 laser for a total of 6 h. Where applicable, an image with the CSU488 laser was taken every 10 min to assess GFP transfection.

### Quantifications of images

To quantify fluorescence intensity or localisation, cells were processed for immunofluorescence with antibodies binding to EGFP, tubulin and CENP-E; 16-bit images were obtained using Airyscan microscopy. To allow comparisons, the same acquisition settings were used for all images in each set of experiments.

AQ11: AQ12: AQ13: AQ14: AQ15:

To quantify the amount of APC-C or APC-C-TBS1 on spindles, EGFP fluorescence intensity was measured in metaphase cells using the ImageJ software (Schneider et al., 2012), in delineated regions of interest (ROIs) on Airyscan images in one focal plane. ROIs were drawn using the 'tubulin' channel: two ROIs in the background ('bck'), two ROIs on hemi-spindles ('sp'), two ROIs on centrosomes ('c'), two ROIs on astral microtubules ('as') and two ROIs in the cytosol ('cy'). The mean fluorescence intensity was measured in ROIs in the 'EGFP' channel and the mean background was subtracted from the mean intensities of each ROI. Fluorescence intensities were then averaged and normalised with respect to the fluorescence intensity on centrosomes.

To quantify colocalisation between EGFP (APC-C or APC-C-TBS1) and CENP-E staining, a macro was created in ImageJ software. First, the mean and standard deviation (s.d.) were measured in the 'EGFP' channel on images of mock-transfected control cells ('bck'). Then, images of cells expressing APC-C or APC-C-TBS1 were processed as follows: the 'CENP-E' channel was bandpass-filtered and the threshold set using RenyEntropy settings; for the 'EGFP' channel, the threshold was set to bck+(4×s.d.). The surfaces of both segmented images and the overlap between them were measured. Colocalisation results are expressed as the ratio (percentage) of the overlap surface to the CENP-E surface.

## Statistics

All statistical analyses were performed using Prism 6 (GraphPad software). The tests performed are specified in the figure legends.

## Miscellaneous

Visualisation of molecular models and generation of structural figures were handled with Chimera (Pettersen et al., 2004). Kymographs were generated by ImageJ software (Schneider et al., 2012). SuperPlots were generated as described in Lord et al. (2020). The TBS1 and TBS2 sequences were submitted for structure prediction to https://robetta.bakerlab.org (Baek et al., 2021).

### Acknowledgements

We thank Annie Andrieux for helpful discussion. This work used the Photonic Imaging Center of Grenoble Institute Neuroscience (Université Grenoble Alpes – Inserm U1216), which is part of the Imagerie en Sciences du Vivant (ISdV) core facility and certified by the Infrastructures en Biologie Santé et Agronomie (IBiSA) label. We thank Yasmina Saoudi for her assistance on the imaging facility. This work used the electron microscopy facilities at the Grenoble Instruct-ERIC Center (ISBG; UAR 3518 CNRS CEA-UGA-EMBL) with support from the French Infrastructure for Integrated Structural Biology and GRAL, a project of the Université Grenoble Alpes graduate school within the Grenoble Partnership for Structural Biology. The IBS Electron Microscope facility is supported by the Auvergne Rhône-Alpes Region, the Fonds Feder, the Fondation pour la Recherche Médicale and GIS-IBiSA. We thank the members of the electron microscope facility for their help.

### Competing interests

The authors declare no competing or financial interests.

### Author contributions

Conceptualization: L.S., A.F.-L., I.A.; Formal analysis: E.D.; Investigation: L.S., J.D., A.V., A.F.-L.; Resources: G.S.; Writing - original draft: L.S., A.F.-L., I.A.; Writing - review & editing: L.S., A.F.-L., I.A.; Funding acquisition: L.S., I.A.

### Funding

This work was supported by the Institut National de la Santé et de la Recherche Médicale (INSERM; French National Institute for Health and Medical Research) and the Centre National de la Recherche Scientifique (CNRS; French National Centre for Scientific Research) through their joint ATIP-Avenir program, and by the Association pour la Recherche sur le Cancer.

### Data availability

Xxxxxxxxxxxxx.

### References

**Akhmanova, A. and Hoogenraad, C. C.** (2015). Microtubule minus-end-targeting proteins. *Curr. Biol.* **25**, R162-R171. doi:10.1016/j.cub.2014.12.027

**Al-Bassam, J., Ozer, R. S., Safer, D., Halpain, S. and Milligan, R. A.** (2002). MAP2 and tau bind longitudinally along the outer ridges of microtubule protofilaments. *J. Cell Biol.* **157**, 1187-1196. doi:10.1083/jcb.200201048

**Almuriekhi, M., Shintani, T., Fahiminiya, S., Fujikawa, A., Kuboyama, K., Takeuchi, Y., Nawaz, Z., Nadaf, J., Kamel, H., Kitam, A. K. et al.** (2015). Loss-of-function mutation in APC2 causes sotos syndrome features. *Cell Rep.* **10**, 1585-1598. doi:10.1016/j.celrep.2015.02.011

**Arnal, I., Heichette, C., Diamantopoulos, G. S. and Chrétien, D.** (2004). CLIP-170/tubulin-curved oligomers coassemble at microtubule ends and promote rescues. *Curr. Biol.* **14**, 2086-2095. doi:10.1016/j.cub.2004.11.055

**Baek, M., DiMaio, F., Anishchenko, I., Dauparas, J., Ovchinnikov, S., Lee, G. R., Wang, J., Cong, Q., Kinch, L. N., Schaeffer, R. D. et al.** (2021). Accurate prediction of protein structures and interactions using a three-track neural network. *Science* **373**, 871-876. doi:10.1126/science.abj8754

**Bahmanyar, S., Nelson, W. J. and Barth, A. I. M.** (2009). Role of APC and its binding partners in regulating microtubules in mitosis. *Adv. Exp. Med. Biol.* **656**, 65-74. doi:10.1007/978-1-4419-1145-2_6

**Bakhoum, S. F., Genovese, G. and Compton, D. A.** (2009). Deviant kinetochore microtubule dynamics underlie chromosomal instability. *Curr. Biol. CB* **19**, 1937-1942. doi:10.1016/j.cub.2009.09.055

**Banks, J. D. and Heald, R.** (2004). Adenomatous polyposis coli associates with the microtubule-destabilizing protein XMCAK. *Curr. Biol.* **14**, 2033-2038. doi:10.1016/j.cub.2004.10.049

**Baumann, S., Komissarov, A., Gili, M., Ruprecht, V., Wieser, S. and Maurer, S. P.** (2020). A reconstituted mammalian APC-kinesin complex selectively transports defined packages of axonal mRNAs. *Sci. Adv.* **6**, eaaz1588. doi:10.1126/sciadv.aaz1588

**Beckers, M. and Sachse, C.** (2020). Permutation testing of Fourier shell correlation for resolution estimation of cryo-EM maps. *J. Struct. Biol.* **212**, 107579. doi:10.1016/j.jsb.2020.107579

**Benoit, M. P. M. H., Asenjo, A. B. and Sosa, H.** (2018). Cryo-EM reveals the structural basis of microtubule depolymerization by kinesin-13s. *Nat. Commun.* **9**, 2748. doi:10.1038/s41467-018-04858-6

**Brouhard, G. J., Stear, J. H., Noetzel, T. L., Al-Bassam, J., Kinoshita, K., Harrison, S. C., Howard, J. and Hyman, A. A.** (2008). XMAP215 Is a Processive Microtubule Polymerase. *Cell* **132**, 79-88. doi:10.1016/j.cell.2007.11.043

**Cheeseman, I. M. and Desai, A.** (2008). Molecular architecture of the kinetochore–microtubule interface. *Nat. Rev. Mol. Cell Biol.* **9**, 33-46. doi:10.1038/nrm2310

**Cook, A. D., Manka, S. W., Wang, S., Moores, C. A. and Atherton, J.** (2020). A microtubule RELION-based pipeline for cryo-EM image processing. *J. Struct. Biol.* **209**, 107402. doi:10.1016/j.jsb.2019.10.004

**Davis, T. N. and Wordeman, L.** (2007). Rings, bracelets, sleeves, and chevrons: new structures of kinetochore proteins. *Trends Cell Biol.* **17**, 377-382. doi:10.1016/j.tcb.2007.08.001

**Deka, J., Kuhlmann, J. and Müller, O.** (1998). A domain within the tumor suppressor protein APC shows very similar biochemical properties as the microtubule-associated protein tau. *Eur. J. Biochem.* **253**, 591-597. doi:10.1046/j.-1432-1327.1998.2530591.x

**Draviam, V. M., Shapiro, I., Aldridge, B. and Sorger, P. K.** (2006). Misorientation and reduced stretching of aligned sister kinetochores promote chromosome missegregation in EB1- or APC-depleted cells. *EMBO J.* **25**, 2814-2827. doi:10.1038/sj.emboj.7601168

**Emsley, P., Lohkamp, B., Scott, W. and Cowtan, F.** (2010). Features and development of coot. *Acta Crystallogr. D Biol. Crystallogr.* **D66**, 486-450. doi:10.1107/S0907444910007493

**Fodde, R., Smits, R. and Clevers, H.** (2001a). APC, signal transduction and genetic instability in colorectal cancer. *Nat. Rev. Cancer* **1**, 55-67. doi:10.1038/35094067

**Fodde, R., Kuipers, J., Rosenberg, C., Smits, R., Kielman, M., Gaspar, C., van Es, J. H., Breukel, C., Wiegant, J., Giles, R. H. et al.** (2001b). Mutations in the APC tumour suppressor gene cause chromosomal instability. *Nat. Cell Biol.* **3**, 433-438. doi:10.1038/35070129

**Green, R. A., Wollman, R. and Kaplan, K. B.** (2005). APC and EB1 function together in mitosis to regulate spindle dynamics and chromosome alignment. *Mol. Biol. Cell* **16**, 4609-4622. doi:10.1091/mbc.e05-03-0259

**Honnappa, S., John, C. M., Kostrewa, D., Winkler, F. K. and Steinmetz, M. O.** (2005). Structural insights into the EB1-APC interaction. *EMBO J.* **24**, 261-269. doi:10.1038/sj.emboj.7600529

**Joseph, A. P., Lagerstedt, I., Jakobi, A., Burnley, T., Patwardhan, A., Topf, M. and Winn, M.** (2020). Comparing Cryo-EM reconstructions and validating atomic model fit using difference maps. *J. Chem. Inf. Model.* **60**, 2552-2560. doi:10.1021/acs.jcim.9b01103

**Juanes, M. A.** (2020). Cytoskeletal control and Wnt signaling—APC's dual contributions in stem cell division and colorectal cancer. *Cancers* **12**, 3811. doi:10.3390/cancers12123811

**Kahn, O. I., Schätzle, P., van de Willige, D., Tas, R. P., Lindhout, F. W., Portegies, S., Kapitein, L. C. and Hoogenraad, C. C.** (2018). APC2 controls dendrite development by promoting microtubule dynamics. *Nat. Commun.* **9**, 2773. doi:10.1038/s41467-018-05124-5

**Kaplan, K. B., Burds, A. A., Swedlow, J. R., Bekir, S. S., Sorger, P. K. and Näthke, I. S.** (2001). A role for the Adenomatous Polyposis Coli protein in chromosome segregation. *Nat. Cell Biol.* **3**, 429-432. doi:10.1038/35070123

**Kapoor, T. M., Lampson, M. A., Hergert, P., Cameron, L., Cimini, D., Salmon, E. D., McEwen, B. F. and Khodjakov, A.** (2006). Chromosomes can congress to the metaphase plate before biorientation. *Science* **311**, 388-391. doi:10.1126/science.1122142

**Kellogg, E. H., Hejab, N. M. A., Poepsel, S., Downing, K. H., DiMaio, F. and Nogales, E.** (2018). Near-atomic model of microtubule-tau interactions. *Science* **360**, 1242-1246. doi:10.1126/science.aat1780

**Lord, S. J., Velle, K. B., Mullins, R. D. and Fritz-Laylin, L. K.** (2020). SuperPlots: Communicating reproducibility and variability in cell biology. *J. Cell Biol.* **219**, e202001064. doi:10.1083/jcb.202001064

**Mills, K. M., Brocardo, M. G. and Henderson, B. R.** (2016). APC binds the Miro/Milton motor complex to stimulate transport of mitochondria to the plasma membrane. *Mol. Biol. Cell* **27**, 466-482. doi:10.1091/mbc.e15-09-0632

**Miranda, J. J. L., De Wulf, P., Sorger, P. K. and Harrison, S. C.** (2005). The yeast DASH complex forms closed rings on microtubules. *Nat. Struct. Mol. Biol.* **12**, 138-143. doi:10.1038/nsmb896

**Mogensen, M. M., Tucker, J. B., Mackie, J. B., Prescott, A. R. and Näthke, I. S.** (2002). The adenomatous polyposis coli protein unambiguously localizes to microtubule plus ends and is involved in establishing parallel arrays of microtubule bundles in highly polarized epithelial cells. *J. Cell Biol.* **157**, 1041-1048. doi:10.1083/jcb.200203001

**Mohn, J. L., Alexander, J., Pirone, A., Palka, C. D., Lee, S. Y., Mebane, L., Haydon, P. G. and Jacob, M. H.** (2014). Adenomatous polyposis coli protein deletion leads to cognitive and autism-like disabilities. *Mol. Psychiatry* **19**, 1133-1142. doi:10.1038/mp.2014.61

**Monda, J. K., Whitney, I. P., Tarasovetc, E. V., Wilson-Kubalek, E., Milligan, R. A., Grishchuk, E. L. and Cheeseman, I. M.** (2017). Microtubule tip tracking by the spindle and kinetochore protein ska1 requires diverse tubulin-interacting surfaces. *Curr. Biol.* **27**, 3666-3675.e6. doi:10.1016/j.cub.2017.10.018

**Moseley, J. B., Bartolini, F., Okada, K., Wen, Y., Gundersen, G. G. and Goode, B. L.** (2007). Regulated binding of adenomatous polyposis coli protein to actin. *J. Biol. Chem.* **282**, 12661-12668. doi:10.1074/jbc.M610615200

**Nakamura, M., Zhou, X. Z. and Lu, K. P.** (2001). Critical role for the EB1 and APC interaction in the regulation of microtubule polymerization. *Curr. Biol.* **11**, 1062-1067. doi:10.1016/S0960-9822(01)00297-4

**Näthke, I. S.** (2006). Cytoskeleton out of the cupboard: Colon cancer and cytoskeletal changes induced by loss of APC. *Nat. Rev. Cancer* **6**, 967-974. doi:10.1038/nrc2010

**Nelson, S. and Näthke, I. S.** (2013). Interactions and functions of the adenomatous polyposis coli (APC) protein at a glance. *J. Cell Sci.* **126**, 873-877. doi:10.1242/jcs.100479

**Nicholls, R. A., Tykac, M., Kovalevsky, O. and Murshudov, G. N.** (2018). Current approaches for the fitting and refinement of atomic models into cryo-EM maps using CCP-EM. *Acta Crystallogr* **D74**, 215-227. doi:0.1107/S2059798318007313

**Okada, K., Bartolini, F., Deaconescu, A. M., Moseley, J. B., Dogic, Z., Grigorieff, N., Gundersen, G. G. and Goode, B. L.** (2010). Adenomatous polyposis coli protein nucleates actin assembly and synergizes with the formin mDia1. *J. Cell Biol.* **189**, 1087-1096. doi:10.1083/jcb.201001016

**Onouchi, T., Kobayashi, K., Sakai, K., Shimomura, A., Smits, R., Sumi-Ichinose, C., Kurosumi, M., Takao, K., Nomura, R., Iizuka-Kogo, A. et al.** (2014). Targeted deletion of the C-terminus of the mouse adenomatous polyposis coli tumor suppressor results in neurologic phenotypes related to schizophrenia. *Mol. Brain* **7**, 21. doi:10.1186/1756-6606-7-21

**Peris, L., Thery, M., Fauré, J., Saoudi, Y., Lafanechère, L., Chilton, J. K., Gordon-Weeks, P., Galjart, N., Bornens, M., Wordeman, L. et al.** (2006). Tubulin tyrosination is a major factor affecting the recruitment of CAP-Gly proteins at microtubule plus ends. *J. Cell Biol.* **174**, 839-849. doi:10.1083/jcb.200512058

**Pettersen, E. F., Goddard, T. D., Huang, C. C., Couch, G. S., Greenblatt, D. M., Meng, E. C. and Ferrin, T. E.** (2004). UCSF Chimera–a visualization system for exploratory research and analysis. *J. Comput. Chem.* **25**, 1605-1612. doi:10.1002/jcc.20084

**Ramey, V. H., Wang, H.-W., Nakajima, Y., Wong, A., Liu, J., Drubin, D., Barnes, G. and Nogales, E.** (2011). The Dam1 ring binds to the E-hook of tubulin and diffuses along the microtubule. *Mol. Biol. Cell* **22**, 457-466. doi:10.1091/mbc.e10-10-0841

**Ramirez-Rios, S., Serre, L., Stoppin-Mellet, V., Prezel, E., Vinit, A., Courriol, E., Fourest-Lieuvin, A., Delaroche, J., Denarier, E. and Arnal, I.** (2017). A TIRF microscopy assay to decode how tau regulates EB's tracking at microtubule ends. *Methods Cell Biol.* **141**, 179-197. doi:10.1016/bs.mcb.2017.06.013

**Ramlaul, K., Palmer, C. M. and Aylett, C. H. S.** (2019). A local agreement filtering algorithm for transmission EM reconstructions. *J. Struct. Biol.* **205**, 30-40. doi:10.1016/j.jsb.2018.11.011

**Rohou, A. and Grigorieff, N.** (2015). CTFFIND4: Fast and accurate defocus estimation from electron micrographs. *J. Struct. Biol.* **192**, 216-221. doi:10.1016/j.jsb.2015.08.008

**Ruane, P. T., Gumy, L. F., Bola, B., Anderson, B., Wozniak, M. J., Hoogenraad, C. C. and Allan, V. J.** (2016). Tumour Suppressor Adenomatous Polyposis Coli (APC) localisation is regulated by both Kinesin-1 and Kinesin-2. *Sci. Rep.* **6**, 1-14. doi:10.1038/srep27456

**Rusan, N. M. and Peifer, M.** (2008). Original CIN: reviewing roles for APC in chromosome instability. *J. Cell Biol.* **181**, 719-726. doi:10.1083/jcb.200802107

**Scheres, S. H. W.** (2015). Semi-automated selection of cryo-EM particles in RELION-1.3. *J. Struct. Biol.* **189**, 114-122. doi:10.1016/j.jsb.2014.11.010

**Schneider, C. A., Rasband, W. S. and Eliceiri, K. W.** (2012). NIH Image to ImageJ: 25 years of image analysis. *Nat. Methods* **9**, 671-675. doi:10.1038/nmeth.2089

**Serre, L., Stoppin-Mellet, V. and Arnal, I.** (2019). Adenomatous polyposis coli as a scaffold for microtubule end-binding proteins. *J. Mol. Biol.* **431**, 1993-2005. doi:10.1016/j.jmb.2019.03.028

**Shemesh, A., Ginsburg, A., Levi-Kalisman, Y., Ringel, I. and Raviv, U.** (2018). Structure, Assembly, and Disassembly of Tubulin Single Rings. *Biochemistry* **57**, 6153-6165. doi:10.1021/acs.biochem.8b00560

**Tan, D., Asenjo, A. B., Mennella, V., Sharp, D. J. and Sosa, H.** (2006). Kinesin-13s form rings around microtubules. *J. Cell Biol.* **175**, 25-31. doi:10.1083/jcb.200605194

**Volkov, V. A.** (2020). Microtubules pull the strings: disordered sequences as efficient couplers of microtubule-generated force. *Essays Biochem.* **64**, 371-382. doi:10.1042/EBC20190078

**Weaver, L. N. and Walczak, C. E.** (2015). Spatial gradients controlling spindle assembly. *Biochem. Soc. Trans.* **43**, 7-12. doi:10.1042/BST20140243

**Wehland, J. and Willingham, M. C.** (1983). A rat monoclonal antibody reacting specifically with the tyrosylated form of alpha-tubulin. II. Effects on cell movement, organization of microtubules, and intermediate filaments, and arrangement of Golgi elements. *J. Cell Biol.* **97**, 1476-1490. doi:10.1083/jcb.97.5.1476

**Zheng, S. Q., Palovcak, E., Armache, J.-P., Verba, K. A., Cheng, Y. and Agard, D. A.** (2017). MotionCor2: anisotropic correction of beam-induced motion for improved cryo-electron microscopy. *Nat. Methods* **14**, 331-332. doi:10.1038/nmeth.4193

**Zumbrunn, J., Kinoshita, K., Hyman, A. A. and Näthke, I. S.** (2001). Binding of the adenomatous polyposis coli protein to microtubules increases microtubule stability and is regulated by GSK3β phosphorylation. *Curr. Biol.* **11**, 44-49. doi:10.1016/S0960-9822(01)00002-1

**Summary:** The C-terminal domain of adenomatous polyposis coli (APC) regulates microtubule dynamics and organises ring-like tubulin oligomers around the microtubule wall, and plays a role in mitotic spindle function.

AQ25

AQ25:

**Funding details**

| S.No. | Funder name | Funder ID | Grant ID |
|---|---|---|---|